Food Hydrocolloids 74 (2018) 1–10

Contents lists available at ScienceDirect

Food Hydrocolloids

journal homepage: www.elsevier.com/locate/foodhyd

Preparation and characterization of iron-alginate beads with some types of iron used in supplementation and fortification strategies

Osmaly Churio [a], Fernando Pizarro [b], Carolina Valenzuela [a, *]

[a] Faculty of Veterinary and Animal Sciences, University of Chile, Santa Rosa 11.735, La Pintana, Santiago, Chile
[b] Micronutrients Laboratory, Institute of Nutrition and Food Technology (INTA), University of Chile, Avda. El Líbano 5524, Santiago, Chile

ARTICLE INFO

Article history:
Received 23 February 2017
Received in revised form
13 July 2017
Accepted 20 July 2017
Available online 24 July 2017

Keywords:
Alginate beads
Delivery
Heme iron
Non-heme iron

ABSTRACT

Our work aimed to develop and characterize different alginate beads with either non-heme iron or a blend of heme/non-heme iron. We chose non-heme iron salts such as ferrous sulfate (FS), ferrous ammonium sulfate (FAS), ferric citrate (FC), ferrous fumarate (FF), and ferrous bis-glycinate chelate (FCH) at different concentrations as a source of iron for our beads. We also chose spray-dried blood cells (SDBC) as a source of heme iron to be mixed with non-heme iron sources for the development of blend beads. FS, FAS and FC did not form beads by the traditional method of external ionic gelation, unlike FF, FCH and their blends with SDBC, which did form beads for every solution concentration. These beads were characterized by iron content, encapsulation efficiency (EE%), size, color, structure by FTIR, morphology, swelling studies and *in vitro* iron release studies. Blend beads showed a spherical shape, more homogeneous surface, high iron content (31.3 ± 1.4 to 61.1 ± 4.4 mg Fe/g dried beads) and high EE% (57.6 ± 7.7% to 78.5 ± 2.9%). Major structural interactions were of hydrophilic nature, for all beads. Under simulated gastric incubation conditions, blend beads showed higher stability and released less iron (11–13%) than FF and FCH-alginate beads (19–23%). Under simulated intestinal incubation conditions, all beads released their iron content over a 3 h period.

1. Introduction

Iron deficiency anemia continues to be the most prevalent nutritional deficiency in the world, affecting about 29% of population (World Health Organization, 2015). This deficiency usually results from insufficient dietary iron intake due to consumption of plant-based diets containing low levels of heme iron (Carpenter & Mahoney, 1992; Heath & Fairweather-Tait, 2002). Bioavailability of heme iron is greater than that from non-heme iron (Conrad & Umbreit, 2000). Nonetheless, fortification and supplementation strategies have been implemented and they have had an important beneficial effect. Yet iron deficiency remains very prevalent in developing countries (Galicia, Grajeda, & López de Romaña, 2016), and these strategies appear to have had little impact until recently (Lynch, 2005). Discontinuation of supplementation therapy or consumption of iron-fortified foods by patients is explained by some of the following reasons: organoleptic problems generating free iron in foods (Douglas, Rainey, Wong, Edmondson, & La Croix, 1981; Hurrell, 2002), decreased bioavailability due to interactions of iron with other components of the diet at the gastrointestinal level (Conrad & Umbreit, 2000), therapy oblivion, low tolerance to iron (Coplin, Schuette, Leichtmann, & Lashner, 1991), and gastrointestinal disorders (Hallberg, Ryttinger, & Solvell, 1966).

Encapsulation technology has brought improvements regarding several of the above mentioned problems. The main encapsulation method used for iron supplementation or fortification strategies is its entrapment in liposomes (Mehansho, 2006; Zimmermann, 2004). However, as liposomes are thermodynamically unstable they will aggregate, fuse, flocculate and precipitate during storage (Zuidam, 2012). In that regards, Kokkona, Kallinteri, Fatouros, and Antimisiaris (2000) state that when faced with intestinal-like conditions i.e. the presence of biliary salts and pancreatin enzymes, liposomes that are composed of lipids with low transition temperatures become highly unstable and release its contents. An alternative to liposomes, the gelation ionic method to form alginate beads has been widely studied in food but sparsely investigated to encapsulate iron forms for supplementation or fortification purposes (Al Gawhari, 2016; Perez-Moral, Gonzalez, & Parker, 2013; Valenzuela, Hernández, Morales, & Pizarro, 2016; Valenzuela,

* Corresponding author. Casilla 2 Correo 15, La Granja, Santiago, Chile.
E-mail address: cvalenzuelav@u.uchile.cl (C. Valenzuela).

http://dx.doi.org/10.1016/j.foodhyd.2017.07.020
0268-005X/

Hernández, Morales, Neira-Carrillo, & Pizarro, 2014). This encapsulation method could be promising as it has exhibited several desired properties in this regard, namely a high encapsulation efficiency for heme iron sources such as spray-dried blood cells (SDBC) (Valenzuela et al., 2014), low iron release in gastric conditions, and high iron release in the duodenal medium (Perez-Moral et al., 2013; Valenzuela et al., 2016).

Spray-dried erythrocytes constitute a good and safe source of heme iron (Toldrà, Elias, Parés, Saguer, & Carretero, 2004) that can be encapsulated by means of ionic gelation, though the iron content of these beads is very low (Valenzuela et al., 2014). This inconvenience however, could be improved upon by their mixture with non-heme iron sources. Among the main kinds of non-heme iron currently used for oral supplementation or fortification strategies we can find ferrous sulfate (which is recognized as the gold standard), other iron salts (such as ferrous gluconate, ferrous fumarate, ferrous lactate, ferric ammonium, ferric citrate), and protected iron in the form of Na-Fe-EDTA and ferrous bis-glycinate chelate (Hurrell, 1997; Mehansho, 2006). In the case of ferrous bis-glycinate chelate, this has been shown to have a higher bioavailability than ferrous sulfate and has also been widely used in oral fortification (Pineda & Ashmead, 2001).

To the best of our knowledge, there have been no studies about the encapsulation of blended heme iron sources with the main sources of non-heme iron that are currently used to prevent iron deficiency anemia. This blend could improve the bioavailability of the resulting formulation and therefore, we have aimed in this study to develop and characterize different alginate beads with either non-heme iron or blends of heme and non-heme iron sources.

2. Material and methods

2.1. Material

Sodium alginate (viscosity of 25.7 cps at 25 °C, 2 g/100 mL solution) was purchased from Sigma-Aldrich, USA, and was used as wall material.

Common supplementation and/or fortification iron salts were used as core material. Non-heme iron salts used were: ferrous sulfate heptahydrate (FS), ferrous ammonium sulfate (FAS), ferric citrate (FC), ferrous fumarate (FF) and ferrous bis-glycinate chelate (Ferrochel®) (FCH). These iron salts were purchased from Merck S.A. with the sole exception of FCH, which was purchased from Albion Laboratories Inc, Clearfield, Utah. Heme iron was sourced from bovine spray-dried blood cells (SDBC) and purchased from Licán Alimentos S.A. This multinational company follows the strictest international hygiene and quality standards (HACCP Codex Alimentarius, GMP, ISO 9001:2008-UKAS) when performing animal blood harvest procedures as well as when processing spray-dried blood cells, which are also subjected to thermal processing (140 °C on entry and 80–90 °C on exit) to reduce any microbial load present in them (Toldrà et al., 2004). This treatment along with the afore mentioned industry certifications allow for this product to be deemed a food ingredient that is safe for human consumption.

Total iron content was determined for all core materials through atomic absorption spectrophotometry techniques. Reagents were all of analytical grade and purchased from Merck S.A. Bile extract and pancreatin (trypsin, amylase, lipase, ribonuclease, and protease) were purchased from Sigma-Aldrich, USA.

2.2. Iron beads preparation

Control beads were prepared without including any iron form in them. Non-heme iron beads were prepared following a three-step procedure: suspending iron salts in a water solution, mixture with a gelification solution, and bead shaping and drying. A sodium alginate solution (2% w/v in deionized water) was chosen as solvent for suspending FS, FAS and FC iron salts at 0.05, 0.1, 0.5 and 1% w/v. On the other hand, FF and FCH salts were suspended at 1, 2 and 3% w/v. Afterwards, these suspensions were collected in a tuberculin syringe and dropped into a gelling solution made from calcium chloride in deionized water (5% w/v). Finally, beads were formed and then deposited in plastic boxes to be dried until reaching a constant weight at a temperature of 40 °C (≈10 h). Once dried, these beads were removed from their boxes and stored at environmental conditions.

As those suspensions based on FS, FAS and FC did not form beads, only FF and FCH were used to prepare blended non-heme/heme iron beads. The same process as outlined above was repeated with the sole difference that a blend of FF and FCH suspensions at 1, 2 and 3% w/v with SDBC at 10% w/v became the basis to prepare the blend beads.

2.3. Appearance and color

Beads appearance was captured with a Sony DSC-HX1 (Sony Corporation, Japan) digital camera, their color was measured and registered on triplicate according to the Hunter Lab color scale (N = 30 for each replicate) with a Konica-Minolta CR-300 (Konica Minolta Inc, Japan) colorimeter.

2.4. Iron content

Beads total iron content was determined through acid digestion (method 999.11) (AOAC, 1996) coupled with an atomic absorption spectrophotometer (GBC, 905AA, Australia). Spectrophotometric measurements were performed on triplicate validated against a standard curve assessed at λ = 248.3 nm, using a commercial iron standard, 1000 μg/mL (J.T. Baker, USA).

2.5. Encapsulation efficiency (EE%)

Following Valenzuela et al. (2014) method, EE% was determined calculating the difference between theoretical iron content of each suspension and the total iron content for beads according to Equation (1).

To determine theoretical iron content, we poured ten drops of each suspension into 10 mL of deionized water and mechanically stirred continuously to homogenize it. These homogenized solutions were then subject to atomic absorption spectrophotometry to measure their iron content.

On the other hand, we proceeded to determine total surface iron of 10 beads which were filtered through a Whatman (N°2) paper filter to remove the gelling solution, and then the cake was dispersed in 10 mL of deionized water. These dispersions were sonicated twice, 20 min each time, using an ultrasonic bath (Elmasonic E08.2011, Germany) and samples were then centrifuged at 2900xg for 10 min. The amount of surface iron released into solution was also quantified through atomic absorption spectrophotometry techniques.

$$EE = \frac{Fe_t - Fe_s}{Fe_t} \times 100 \quad (1)$$

where: EE is encapsulation efficiency, Fe_t is the encapsulated theoretical iron and Fe_s is the amount of total surface iron.

2.6. Size

Diameter size for dry beads was measured on triplicate (N = 40 by each replicate) with a Veto E5010109 digital micrometer (Veto & Co, China).

2.7. Fourier transform infrared spectroscopy (FTIR)

FTIR analyses were performed on FF and FCH powders, sodium alginate and some dry beads (FF 3%, FCH 3%, and their respective blends with SDBC). An ATR/FTIR interspec 200-X spectrometer (Interspectrum OU, Estonia) provided FTIR spectra for each one of the analytes.

Spectroscopic measurements on beads samples were performed directly using the PIKE Miracle TM accessory in a Ge single reflection crystal plate. A concave tip was used for all FTIR spectra. An average of 20 scans over the spectral range of 600 to 4000 cm^{-1} yielded each spectra.

2.8. Morphology

Surface morphology of beads was observed with a LEO 1420 VP (Cambridge, UK) scanning electron microscopy (SEM) running on an accelerating voltage of 25 kV. Prior to examination, samples were dehydrated by subjecting them to an acetone series and a critical point dryer. Then they were mounted and fixated with double-sided tape to a cylindrical aluminum stub. Beads were then gold-sputter-coated twice at 20 kV in an argon atmosphere (PELCO 91000, Ted Pella, Inc., USA).

For transmission electron microscopy (TEM) imaging, dried beads were prepared for this procedure by fixating them in 2.5% of glutaraldehyde in sodium cacodylate buffer 0.1 M at pH 7.0. Then dehydrated by immersing them in 50, 70, 95, and 100% ethanol solutions for 15 min in each one and embedded in epoxy resin:-ethanol (1:1) overnight. Afterwards, they were included in the epoxy resin alone (polymerized at 60 °C for 24 h). Thin sections were sliced from these samples with a Sorvall MT-5000 ultramicrotome, stained with aqueous uranyl acetate 1% for 1 min and finally observed with a Philips Tecnai 12 BioTwin Transmission Electron Microscope (FEI Company, The Netherlands) operated at 80 kV. Photographs were processed through a Megaview G2 Snapshot software.

2.9. Swelling studies

One gram of dry beads was placed on a stainless steel grid and then immersed in a plastic petri dish containing either 20 mL of gastric fluid (refer to release studies section) or a phosphate buffer saline (PBS) medium adjusted to pH 6 with HCl 1N at 37 °C. After resting 1 h in gastric fluid or 3 h in PBS medium, beads were gently wiped with paper, weighed in and their weight registered. Their weight change percentage was calculated according to Equation (2).

$$Weight\ change = \left(\frac{FW - IW}{IW}\right) \times 100 \quad (2)$$

where: FW is final weight, IW is initial weight.

After finishing incubating beads in either gastric fluids or PBS solution, these were sampled (N = 15) and processed for SEM imaging to observe their morphology.

2.10. In vitro iron release studies

Human gastric and intestinal conditions were simulated *in vitro* to study iron release. To simulate gastric conditions, we made a solution containing 2 g/L of NaCl and 10 g/L of pepsin that was then adjusted to reach pH 2.0 by adding HCl 1N solution as needed. Next, 1 g of beads were mixed in 100 mL of this suspension, incubated for 1 h at 37 °C and constantly agitated at 150 oscillations/min. On the other hand, intestinal conditions were simulated by dissolving 50 g/L of pancreatin and 31.2 g/L of bile extract in a solution containing 8.76 g/L NaCl and PBS 0.1 M at pH 7.4. Solution's pH was adjusted to 6.0 by adding HCl 1 N as needed.

Beads from simulated gastric incubation were filtered out through a strainer and dried up on absorbent paper. Next, they were incubated in 100 mL of simulated intestinal suspension for 3 h at 37 °C while being constantly agitated at 150 oscillations/min. We measured the total iron that was being released from the beads into the solution at each step. For the simulated gastric incubation we took 5 mL aliquots every 15 min over 1 h and for the simulated intestinal conditions we also took 5 mL aliquots but they were spaced every 20 min over 3 h. These procedures were done in triplicate and total iron content was measured with atomic absorption spectroscopy techniques.

After 60 min of the intestinal incubation had elapsed, beads were drained and dried up on adsorbent paper and then processed for SEM imaging observation.

2.11. Statistical analysis

An ANOVA and a Tukey test ($p < 0.05$) were chosen for the statistical analysis of iron content, EE (%), color, swelling (%) and iron release (%). For beads size comparison analysis, on the other hand, we chose the Kruskal-Wallis and all-pairwise tests ($p < 0.05$).

As for the iron released over the simulated gastric and intestinal incubations, these measurements were graphed using the Microsoft Excel 2010 software (Microsoft Corporation, USA) and then calculated the best-fit trend line, regression equation and R^2 value.

All statistical analyses were run on the Statgraphics Plus 5 software (Statpoint Technologies, Inc., USA).

3. Results and discussion

3.1. Bead shaping

The ionic gelation technique we chose allowed forming spherical droplets which in turn result in spherical particles. However the conventional external ionic gelation method we used did not yield well formed beads in the case of FS (Fig. 1B), FAS (Fig. 1C), and FC (Fig. 1D) for any ratio when compared against our control beads (Fig. 1A). In fact, FS, FAS, and FC suspensions generated very amorphous beads when we used them in low concentration (0.05%), and at greater concentrations (0.1–1%) they turned into a viscous paste. A similar observation has been reported by Perez-Moral et al. (2013) for beads made following this method on several salts such as ferrous gluconate dihydrate, ferrous sulphate heptahydrate, ferric ammonium citrate and ferric chloride alginate. Alginate interactions with iron ions is not well understood yet, but these authors proposed that Fe^{2+} and Ca^{2+} ions compete for binding points within the alginate beads. Another possible explanation in the case of FS could be that, though calcium alginate can encapsulate metal ions it cannot encapsulate anionic species such as FS sulfate groups. This would be due to anionic groups having the same charge as alginate's guluronic acid blocks (Banerjee, Nayak, & Lahiri, 2007).

FF (Fig. 1E) and FCH (Fig. 1G) suspensions at all ratios as well as their blends with SDBC (Fig. 1F and H) formed oblong beads immediately after being dropped into the gelling solution.

Han, Guenier, Salmieri, and Lacroix (2008) also reported FF

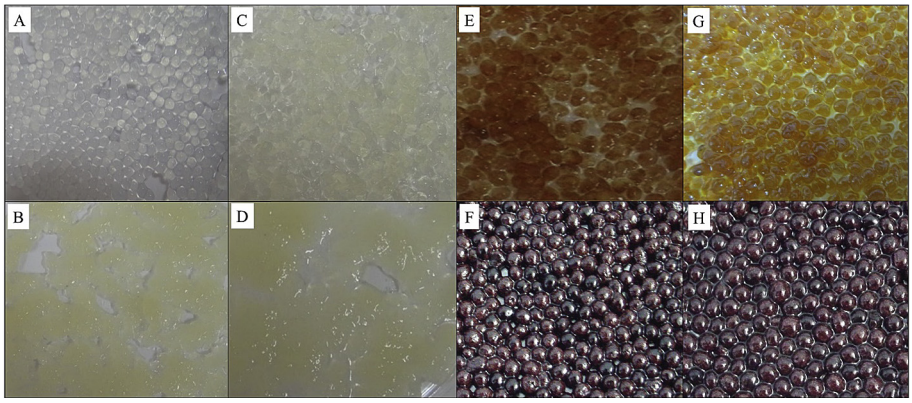

Fig. 1. Digital photographs displaying overall physical appearance for beads of experimental groups alginate control (A), FS 0.05% (B), FAS 0.05% (C), FC 0.05% (D), FF 3% (E), FF 3% plus SDBC (F), FCH 3% (G) and FCH 3% plus SDBC (H).

encapsulation in calcium alginate and chitosan native or functionalized matrix by ionic gelation method. These authors described that the encapsulation process strongly increased stability of FF.

As for the blend beads, their spherical shape was similar to SDBC beads elaborated by Valenzuela et al. (2014) and their appearance was more homogeneous than that of plain FF and FCH beads.

3.2. Characterization of the beads

Table 1 summarizes some bead characteristics. As expected, iron content increased accordingly with FCH and FF salt concentration for each experimental solution. Addition of SDBC to any solution did not significantly increased iron content in blend beads when compared to plain beads. FF beads had a greater iron content but this was simply due to the greater intrinsic iron content in FF (16.2 g Fe/100 g FF) when compared against FCH (10.1 g Fe/100 g FCH). Adding SDBC to formulations did not increased iron content as it only provides 0.24 g Fe per 100 g of product (Valenzuela et al., 2014) and only a low proportion (10%) of it was added to the solution. SDBC is made from whole erythrocytes as a source of heme iron instead of being an extract of hemin or pure heme iron. Bead iron contents were similar to the lowest range reported by Perez-Moral et al. (2013), who created beads from different iron compounds and found iron contents ranging between 50 and 450 mg of iron per g of dried beads. These beads were not made following the conventional external ionic gelation method we used in our study, but instead through an alternate route where iron was included on the cross-linking bath. Our beads though, did have greater iron content than those made by Banerjee et al. (2007) by dissolving $FeCl_3$ in the reticulating solution. These beads contained between 12 and 37 mg of iron per g of wet alginate beads.

EE% for all beads was high but some beads showed a significant trend for a decreasing EE% proportionally to the increase in their core material. The highest EE% was found in blend beads made from FCH 1% + SDBC (Table 1). These values are similar to those reported by Valenzuela et al. (2014) for SDBC-alginate beads, whose EE% ranged from 60 to 76%. This lower EE% values for beads with greater amounts of material in their nucleus has also been reported by other authors (Das, Kasoju, & Bora, 2010). As stated by Chan (2011) this is due to a disproportion between core and bead wall material. This reduced alginate concentration provides fewer binding sites for Ca^{2+} ions which in turn, results in a less compact gel mesh being formed that finally leads to wall collapse and smaller EE% values.

Bead size did not vary for the different kinds of iron salts. Nonetheless, there was a significant size increase for all beads including SDBC as this product is quite voluminous. Which is consistent with the experience of Valenzuela et al. (2014), who stated that SDBC bead's size significantly increased proportionally to their SDBC content.

Regarding bead color, those made from FF (Fig. 1E) were a darker shade of brown than those made from FCH (Fig. 1G). This visual judgment mirrored the results of their color analysis, where *L*, *a* and *b* parameters exhibited different values (Table 1). Similarly, SDBC blend beads were regarded as an even darker shade of brown but their colorimetric values were not significantly different among the

Table 1
Iron content, encapsulation efficiency, size and bead colorimetric values for different sources of iron by iron concentration level in dry beads.

Iron source	%	Fe content (mg/g)	EE (%)	Size (mm)	Color		
					L	a	b
FF	1%	40.9 ± 2.2^{ab}	73.7 ± 6.7^{a}	0.82 ± 0.11^{a}	17.8 ± 3.4^{a}	1.1 ± 0.6^{a}	1.2 ± 0.3^{a}
	2%	56.3 ± 9.9^{cb}	68.2 ± 8.9^{a}	$0.87 \pm 0.17^{a,b,c}$	18.4 ± 2.1^{a}	1.2 ± 0.5^{a}	1.3 ± 0.2^{a}
	3%	61.1 ± 4.4^{c}	57.6 ± 7.7^{b}	$0.85 \pm 0.15^{a,b}$	18.1 ± 2.2^{a}	1.4 ± 0.4^{a}	1.4 ± 0.2^{a}
FCH	1%	31.4 ± 7.9^{a}	74.7 ± 11.1^{a}	$0.87 \pm 0.21^{a,b}$	14.4 ± 0.5^{b}	3.3 ± 0.3^{b}	2.1 ± 0.5^{b}
	2%	40.0 ± 6.4^{ab}	70.3 ± 6.4^{a}	0.82 ± 0.17^{a}	13.2 ± 0.3^{b}	3.7 ± 0.1^{b}	2.5 ± 0.4^{b}
	3%	51.1 ± 3.7^{cb}	60.6 ± 10.4^{a}	0.82 ± 0.15^{a}	14.1 ± 0.8^{b}	3.5 ± 0.2^{b}	2.2 ± 0.6^{b}
FF + SDBC 10%	1%	43.1 ± 2.5^{ab}	71.2 ± 5.6^{a}	$0.99 \pm 0.18^{c,d}$	22.3 ± 0.9^{c}	1.0 ± 0.2^{c}	0.9 ± 0.2^{c}
	2%	49.7 ± 6.0^{cb}	68.1 ± 8.9^{a}	$0.95 \pm 0.17^{b,c,d}$	25.4 ± 1.8^{c}	1.1 ± 0.2^{c}	0.8 ± 0.4^{c}
	3%	58.8 ± 17.0^{c}	56.0 ± 8.1^{b}	1.08 ± 0.22^{d}	24.6 ± 2.3^{c}	1.2 ± 0.2^{c}	1.0 ± 0.3^{c}
FCH + SDBC 10%	1%	31.3 ± 1.4^{a}	78.5 ± 2.9^{c}	1.09 ± 0.29^{d}	24.8 ± 2.3^{c}	1.0 ± 0.3^{c}	0.8 ± 0.5^{c}
	2%	39.5 ± 3.9^{ab}	70.8 ± 5.3^{a}	$1.00 \pm 0.27^{b,c,d}$	22.2 ± 2.1^{c}	1.2 ± 0.1^{c}	0.9 ± 0.6^{c}
	3%	53.5 ± 6.7^{cb}	62.5 ± 8.7^{a}	1.04 ± 0.18^{d}	23.8 ± 3.5^{c}	1.3 ± 0.4^{c}	1.1 ± 0.4^{c}

a, b, c, d: Different superscript letters within a column indicate significantly different means ($p < 0.05$). EE: encapsulation efficiency.

different kinds of blend beads. All of these color variations are mostly due to the core material as pure alginate beads are translucent (Fig. 1A) while FF and FCH salts are dark brown and SDBC is red/dark brown.

3.3. Structural analysis

3.3.1. FTIR

We analyzed beads' FTIR spectra to characterize potential interactions. Fig. 2A presents FTIR spectra for both wall and core materials (sodium alginate, FF, FCH, SDBC). Fig. 2B shows two distinct frequency regions that constituted the basis for these analyses. All beads exhibited a similar peak to sodium alginate at around 3400 cm^{-1} (region 1), which was more evident and acute in FF and FCH beads. This is indicative of stretching O-H bonds vibrations (Van Hoogmoed, Busscher, & de Vos, 2003), which in turn means that the interaction between all bead's components created a new material as the FTIR spectra for the core materials in this zone are very different.

In the case of SDBC's spectrum, we observed a narrow band at 2953 cm^{-1}, which relates to a stretching vibration in C-H bonds of aliphatic chains (CH_2, CH_3) due to hydrophobic interactions (Valenzuela et al., 2014). This band is not present in blend beads' spectra, therefore indicating that they were formed mainly through hydrophilic interactions.

Sodium alginate shows a typical peak at 1615 cm^{-1} (region 2 in Fig. 2B) that has been identified due to its asymmetric stretching vibrations (C-O) of carboxylate salt ion (Van Hoogmoed et al., 2003). This band tends to fuse with others that are present in FF beads' spectra but is clearly distinguishable in FCH beads' spectra. Among these two, the latter resembled more closely sodium alginate's spectrum.

The more pronounced bands in region 2 of blend beads' spectra belong to SDBC (1650 and 1537 cm^{-1}). The amide I band in SDBC's spectra is due to stretching vibrations of C=O bonds while the amide II results from bending of N-H bonds. This region involves proteins and signals the presence of hemoglobin in SDBC (Valenzuela et al., 2014). Blend beads containing FCH again resembled more closely their original material (SDBC in this case).

Another typical band, though less noticeable, within sodium alginate's spectrum lies at 1413 cm^{-1} and is generated by a symmetric stretching of COO^- groups (Van Hoogmoed et al., 2003). This band vanishes in FF beads' spectra, it is quite similar to sodium alginate's spectrum in FCH beads' spectra, and can also be detected in blend beads' spectra.

We also found another peak in sodium alginate's spectrum at 1116 cm^{-1} but it was not noticed in beads' spectra. This band reflects a stretching of the C-O bonds in ether and alcoholic groups.

On the other hand, FF's spectrum revealed many peaks however, none of them could be detected within the spectra for either FF beads or blended FF beads.

In summary, we draw the following conclusions after comparing

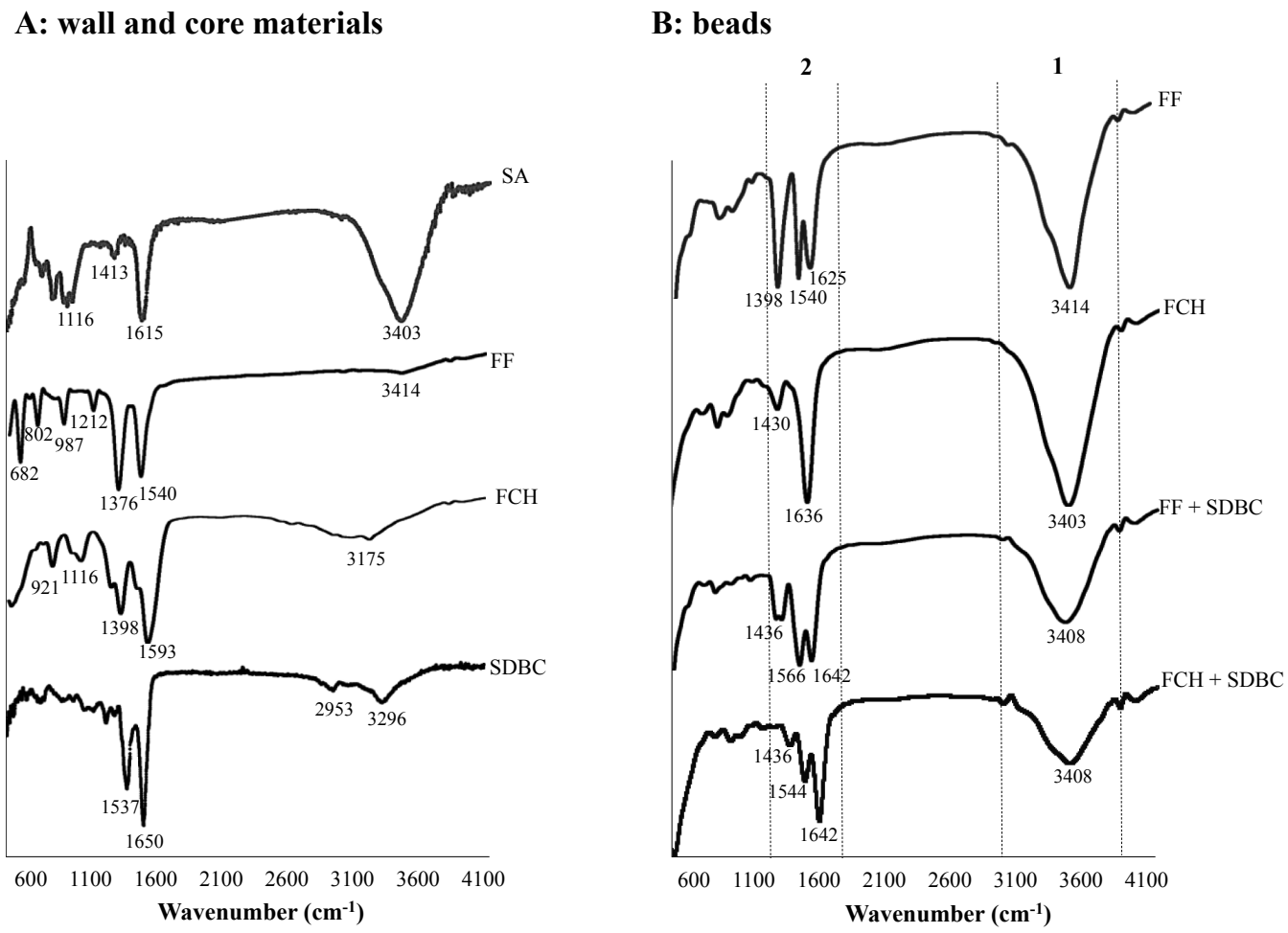

Fig. 2. A: FTIR spectra for materials used to build bead wall and as bead core such as sodium alginate (SA), ferrous fumarate (FF), ferrochel (FCH) and spray-dried blood cells (SDBC). B: FTIR spectra for whole beads from experimental groups FF 3%, FCH 3%, FF 3% + SDBC and FCH 3% + SDBC.

curves for beads against their core materials: 1) marked peaks representing O-H bond stretching in all beads suggests strong hydrophilic interaction are the main drivers behind bead formation, and 2) characteristic FCH spectrum bands were not preserved in beads containing this compound in their core, which indicates that FCH did not induce subsequent modifications in alginate bead structure.

3.3.2. Microstructure

SEM micrographs of dry beads in Fig. 3 reveal irregularly shaped beads (Fig. 3A1 and A2) and a rougher, more heterogeneous surface (Fig. 3A2 and B2) for FF and FCH beads than for blend beads. As it can be observed in Fig. 3C1 and D1, the latter presented a spherical shape and a smooth surface (Fig. 3C2 and D2). Adding SDBC to produce blend beads improved their appearance and microstructure by reducing their roughness and undulations. This is consistent with reports from Valenzuela et al. (2014) who found that SDBC-alginate beads' surface was smooth up until a 1:5 w/w ratio of alginate:SDBC. A spherical shape and a similar surface was also observed by Banerjee et al. (2007) for FeCl3-Ca-alginate beads. Han et al. (2008), meanwhile, reported a smoother surface in alginate-chitosan functionalized beads *vs* native alginate beads, which showed rough, granular and undulating surfaces. These authors state that a denser and more homogeneous structure is observed when there are less hydrophilic interactions. This could explain our observations, as the FTIR analysis (Fig. 2B) shows that FF and FCH beads present sharper peaks with greater surface area in the O-H bonds stretching zone, therefore indicating a greater presence of hydrophilic interactions between the different compounds.

When analyzing our TEM images, we noticed that beads contained the core material, which is darker, between the alginate chains. TEM images also confirmed high agglomeration of iron salts in some parts, mostly in FF beads (Fig. 5E).

3.4. Swelling and iron release behavior at in vitro conditions

Fig. 4 depicts weight change for beads after being subjected to gastric and PBS conditions. We found that FF and FCH beads lost weight in a similar manner (−32 to −44%) for all concentrations when they were subjected to gastric conditions. This outcome was expected due to the well known shrinkage phenomenon that occurs in acidic environments (pH < 4) where, as alginate's carboxylate groups become protonated, the electrostatic repulsion among these groups weakens and favors shrinkage (Pasparakis & Bouropoulos, 2006). Fig. 4A shows microstructure changes. Specifically, we observe how shrinkage and weight loss resulted in a greater amount of undulations on the surface of FF beads than on native beads (Fig. 3 A2).

Blend beads, on the contrary, did not lose weight. Instead, all of them showed some degree of swelling in between 52 and 60% greater than their original mass. Unlike the shrinkage phenomenon, this outcome was not expected as Valenzuela et al. (2016) had previously reported 9–40% of weight loss for SDBC-alginate beads. Nonetheless, these authors observed that weight loss dropped significantly as SDBC content increased. Based on these results, we suspect that mixing different kinds of iron sources could change the swelling pattern for beads under gastric conditions, bringing about consequences on their ability to release iron. Swelling was also

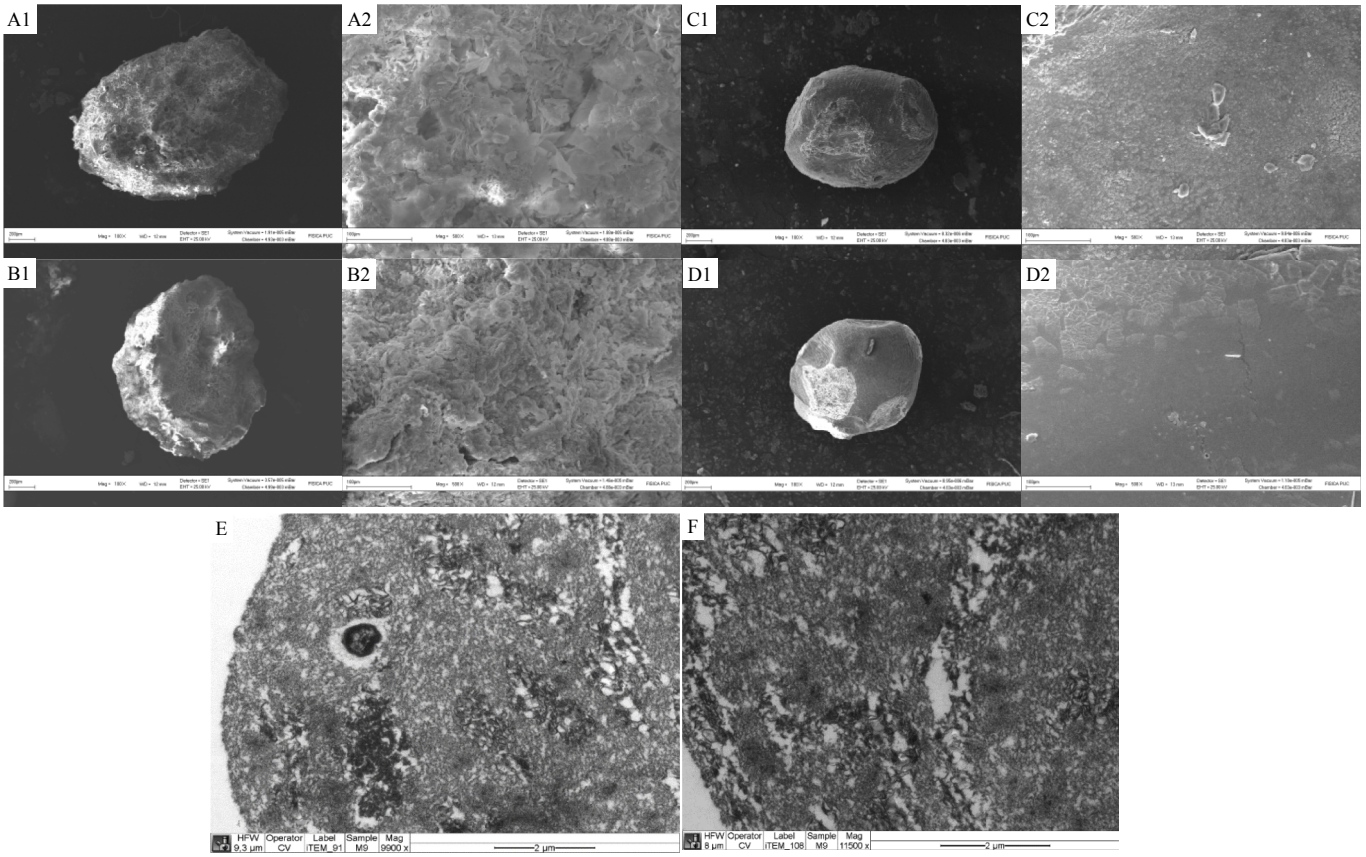

Fig. 3. SEM images of whole beads (1) and bead surface (2) for experimental groups FF 3% (A), FCH 3% (B), FF 3% plus SDBC (C) and FCH 3% plus SDBC (D). E and F: TEM images for beads of experimental groups FF 3% (E) and FF 3% plus SDBC (F).

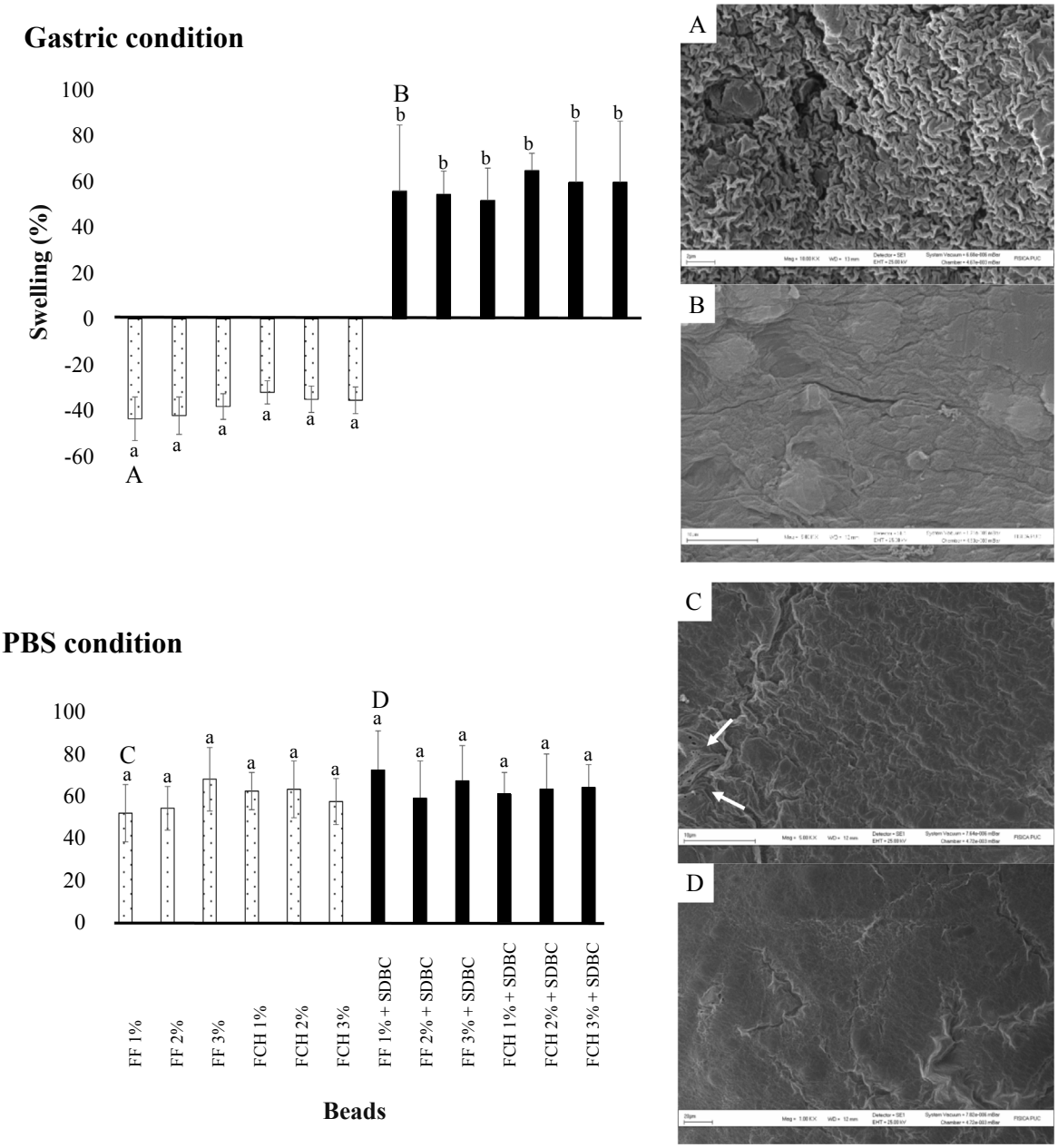

Fig. 4. Bead swelling under simulated gastric incubation and PBS incubation conditions. Uppercase A, B, C and D letters on some columns in the bars charts indicate the source groups for those beads pictured in SEM images A, B, C and D, respectively. Different superscript letters indicate statistically significant differences ($p < 0.05$). A, B, C and D: SEM images of selected beads for both simulated gastric incubation (A and B) and PBS incubation (C and D) conditions.

reported by Anal, Bhopatkar, Tokura, Tamura, and Stevens (2003) for bovine serum albumin-alginate beads during incubation in simulated gastric fluid (pH 1.2). They even noticed that swelling increased significantly as chitosan was added to formulations. Other authors have also reported changes to beads' swelling ability when other polymers have been added to their formulations (Pasparakis & Bouropoulos, 2006). What kind of changes will be observed depends on what molecules are being incorporated and their interactions with those polymers that were already present in the original formulation.

When comparing the surface of blend beads (Fig. 4B) against those without SDBC (Fig. 4A) there is a clear difference. The former presents a smooth, homogeneous surface that is devoid of undulations or pores, which in turn could be an advantage regarding their iron release behavior. Something similar was found for FCH blend beads (pictures not shown).

On PBS incubation all beads behaved similarly, increasing their weight in a range from 52 to 73%. Bead microstructure surface differences were less evident than under gastric conditions, though we must highlight that in the case of FF and FCH beads (picture not shown) we began to notice small pores (white arrows on Fig. 4C). These pores were not found when we inspected images of blend beads. This fact is important because one of the mechanisms for nucleus material diffusion from within alginate beads, is known to be the progressive dissolution of the wall material through the development of pore channels (Gombotz & Wee, 1998).

Regarding beads' iron release behavior, Fig. 5 shows that under gastric conditions, FF and FCH beads release iron in a similar range (19–23%) for all their concentrations, though they almost double the amount of iron released by blend beads (11–13%). Blend beads also showed no significant differences in this behavior among themselves. Iron release curves under gastric incubation tended to be second degree polynomials for all beads. FF and FCH beads exhibited quite similar slopes among them and high R^2 values (0.96–0.99). These slopes were higher than those of blend beads, which also presented high R^2 values (0.97–0.99) and indicate different iron release behaviors among beads (data not shown).

These results could be explained by the morphological differences among beads we determined through SEM imaging and swelling behavior, as previously discussed. Our results are similar to those reported by Valenzuela et al. (2016), who reported an iron release range of 10–25% for SDBC-alginate beads under gastric conditions. Meanwhile Han et al. (2008) reported gastric iron release levels close to 10% for ferrous fumarate-alginate/chitosan beads. However, our results were quite lower than the 45% iron release level reported by Perez-Moral et al. (2013) for iron-alginate beads under gastric conditions (1 h). These authors though, could not encapsulate iron salts by the external ionic gelation method that we were able to apply in this study. This method could have influenced the greater stability shown by our beads under gastric conditions.

Iron release under intestinal conditions was similar for all beads (Fig. 5), reaching almost 100% after 3 h of incubation. Unlike under

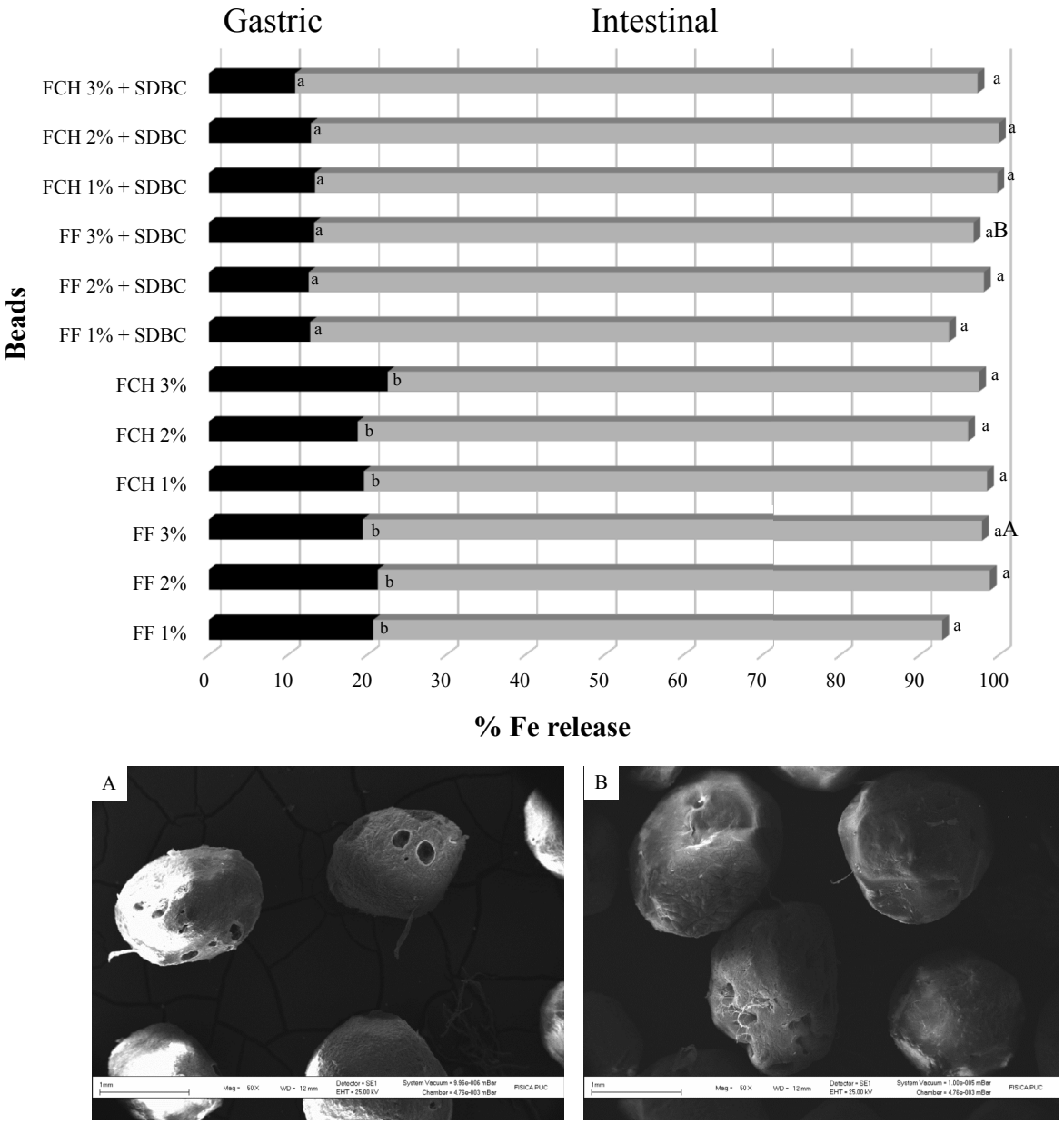

Fig. 5. Total iron release after incubating beads in simulated gastric and intestinal conditions. Uppercase A and B letters on the right side of the stacked bars chart indicate the source groups for those beads pictured in SEM images A and B. Different superscript letters indicate statistically significant differences ($p < 0.05$). A and B: SEM images of selected beads after 60 min under simulated intestinal incubation.

gastric incubation, beads under intestinal conditions presented third degree polynomial curves with similar slopes (data not shown). Proportionally, blend beads released a greater amount of iron as they had lost lower quantities of iron during the gastric incubation. After 60 min of intestinal incubation we noticed through SEM imaging that large pores and cracks began to appear in all beads (Fig. 5A and B). Pore formation has been reported by several authors after completing gastric and intestinal incubations for alginate-beads, and is one of the main paths for this kind of beads to disintegrate and surrender their nucleus material (Gombotz & Wee, 1998; Valenzuela et al., 2016).

After intestinal incubation finished, FF and FCH beads released 25 to 48 mg of iron per gram of beads. In the case of blend beads, this range was of 27–47 mg of iron per gram of beads. These values are greater than what Perez-Moral et al. (2013) reported for iron-alginate beads (6 mg iron per g of dry beads).

Complete disintegration by progressive dissolution of all beads was observed within 150–180 min.

These results are quite promising for oral iron supplementation and fortification, as it is ideally expected for this mineral to be protected at the gastric level and therefore avoid oxidation reactions that turn iron insoluble, decreasing its bioavailability (Annibale, Capurso, & Delle Fave, 2003; Coplin et al., 1991). Another expectation for any encapsulations system is the ability to release its contents within the duodenum, hopefully over a long period of time.

Using heme iron within beads presents advantages due to both its greater bioavailability when compared against non-heme iron, as well as its potentiating effect over non-heme iron absorption (Conrad & Umbreit, 2000). Recently, our research group reported on our finding that erythrocyte stroma is the only factor that increases bioavailability for heme iron (Pizarro et al., 2016). Therefore, encapsulating erythrocytes could lead to increased iron absorption rates. Additionally, Conrad and Umbreit (2000) reported that both heme and non-heme iron are absorbed through different intestinal receptors (Heme Carrier Protein 1 for heme iron cf. Divalent Metal Transporter 1 for non-heme iron), which could be another factor increasing bioavailability of any supplement that combines both types of iron sources. Based on this information, blend beads could be better options to develop potential iron supplements. Proving their efficacy though, would require performing *in vivo* bioavailability assays.

It is important to bear in mind though, that using bovine erythrocytes may carry a risk for transmission of some prion proteins that could cause transmissible spongiform encephalopathies. Considering as well that procedures aimed to eliminate pathogenic bacteria are not effective against prions (Safar, Roller, Gajdusek, & Gibbs, 1993), we strongly recommend that bovine erythrocytes should be sourced from animals that have been certified to be prion-free.

4. Conclusions

We were able of encapsulating several different iron sources that are used in iron supplementation and fortification strategies. Through an external ionic gelation method, some kinds of non-heme iron such as FF and FCH salts as well as heme iron (SDBC) either pure or blended, were successfully encapsulated in alginate beads. These beds contained high levels of iron, high encapsulation efficiency and were able to withstand gastric incubation conditions while only releasing low amounts of iron in this environment. Most of the iron contents were released in intestinal incubation conditions resembling those from the duodenum, which is the target site for absorption of the different kinds of iron we used in our experiment.

Funding

This work was supported by FONDECYT de Iniciación 11140249.

References

Al Gawhari, F. (2016). Preparation of ferrous sulfate microcapsules as a sustained release dosage forms. *International Journal of Applied Pharmaceutics, 8*, 1–4.
Anal, A. K., Bhopatkar, D., Tokura, S., Tamura, H., & Stevens, W. F. (2003). Chitosan-alginate multilayer beads for gastric passage and controlled intestinal release of protein. *Drug Development and Industrial Pharmacy, 29*, 713–724.
Annibale, B., Capurso, G., & Delle Fave, G. (2003). The stomach and iron deficiency anaemia: A forgotten link. *Digestive and Liver Disease, 35*, 288–295.
AOAC. (1996). *Official methods of analysis of the association of official analytical chemists* (16th ed.). Gaithersburg: AOAC International.
Banerjee, A., Nayak, D., & Lahiri, S. (2007). A new method of synthesis of iron doped calcium alginate beads and determination of iron content by radiometric method. *Biochemical Engineering Journal, 33*, 260–262.
Carpenter, C. E., & Mahoney, A. W. (1992). Contributions of heme and non-heme iron to human nutrition. *Critical Reviews in Food Science and Nutrition, 31*, 333–367.
Chan, E. (2011). Preparation of Ca-alginate beads containing high oil content: Influence of process variables on encapsulation efficiency and bead properties. *Carbohydrate Polymers, 84*, 1267–1275.
Conrad, M. E., & Umbreit, J. N. (2000). Iron absorption and transport-an update. *American Journal of Hematology, 64*, 287–298.
Coplin, M., Schuette, S., Leichtmann, G., & Lashner, B. (1991). Tolerability of iron: A comparison of bis-glycino iron II and ferrous sulfate. *Clinical Therapeutics, 13*, 606–612.
Das, R. K., Kasoju, N., & Bora, U. (2010). Encapsulation of curcumin in alginate-chitosan-pluronic composite nanoparticles for delivery to cancer cells. *Nanomedicine: Nanotechnology, Biology and Medicine, 6*, 153–160.
Douglas, F., Rainey, N., Wong, N., Edmondson, L., & La Croix, D. (1981). Color, flavor, and iron bioavailability in iron-fortified chocolate milk. *Journal of Dairy Science, 64*, 1785–1793.
Galicia, L., Grajeda, R., & López de Romaña, D. (2016). Nutrition situation in Latin America and the Caribbean: Current scenario, past trends, and data gaps. *Revista Panamericana de Salud Pública, 40*, 104–113.
Gombotz, W. R., & Wee, S. (1998). Protein release from alginate matrices. *Advanced Drug Delivery Reviews, 31*, 267–285.
Hallberg, L., Ryttinger, L., & Solvell, L. (1966). Side-effects of oral iron therapy. A doubleblind study of different iron compounds in tablet form. *Acta Medica Scandinavica, 459*, 3–10.
Han, J., Guenier, A.-S., Salmieri, S., & Lacroix, M. (2008). Alginate and chitosan functionalization for micronutrient encapsulation. *Journal of Agricultural and Food Chemistry, 56*, 2528–2535.
Heath, A. L. M., & Fairweather-Tait, S. (2002). Clinical implications of changes in the modern diet: Iron intake, absorption and status. *Best Practice & Research Clinical Haematology, 15*, 225–241.
Hurrell, R. (1997). Preventing iron deficiency through food fortification. *Nutrition Reviews, 55*, 210–222.
Hurrell, R. (2002). How to ensure adequate iron absorption from iron-fortified food. *Nutrition Reviews, 60*, 7–15.
Kokkona, M., Kallinteri, P., Fatouros, D., & Antimisiaris, S. G. (2000). Stability of SUV liposomes in the presence of cholate salts and pancreatic lipases: Effect of lipid composition. *European Journal of Pharmaceutical Sciences, 9*, 245–252.
Lynch, S. (2005). The impact of iron fortification on nutritional anaemia. *Best Practice & Research Clinical Haematology, 18*, 333–346.
Mehansho, H. (2006). Iron fortification technology development: New approaches. *Journal of Nutrition, 136*, 1059–1063.
Pasparakis, G., & Bouropoulos, N. (2006). Swelling studies and in vitro release of verapamil from calcium alginate and calcium alginate–chitosan beads. *International Journal of Pharmaceutics, 323*, 34–42.
Perez-Moral, N., Gonzalez, M., & Parker, R. (2013). Preparation of iron-loaded alginate gel beads and their release characteristics under simulated gastrointestinal conditions. *Food Hydrocolloid, 31*, 114–120.
Pineda, O., & Ashmead, H. D. (2001). Effectiveness of treatment of iron-deficiency anemia in infants and young children with ferrous bis-glycinate chelate. *Nutrition, 17*, 381–384.
Pizarro, F., Olivares, M., Valenzuela, C., Brito, A., Weinborn, V., Flores, S., et al. (2016). The effect of proteins from animal source foods on heme iron bioavailability in humans. *Food Chemistry, 196*, 733–738.
Safar, J., Roller, P., Gajdusek, D., & Gibbs, C. J. (1993). Thermal stability and conformational transitions of scrapie amyloid (prion) protein correlate with infectivity. *Protein Science, 2*, 2206–2216.
Toldrà, M., Elias, A., Parés, D., Saguer, E., & Carretero, C. (2004). Functional properties of a spray-dried porcine red blood cell fraction treated by high hydrostatic pressure. *Food Chemistry, 88*, 461–468.
Valenzuela, C., Hernández, V., Morales, S., Neira-Carrillo, A., & Pizarro, F. (2014). Preparation and characterization of heme iron-alginate beads. *LWT- Food Science and Technology, 59*, 1283–1289.
Valenzuela, C., Hernández, V., Morales, S. M., & Pizarro, F. (2016). Heme iron release from alginate beads at *in vitro* simulated gastrointestinal conditions. *Biological*

Trace Element Research, 172, 251–257.
Van Hoogmoed, C. G., Busscher, H. J., & de Vos, P. (2003). Fourier transform infrared spectroscopy studies of alginate–PLL capsules with varying compositions. *Journal of Biomedical Materials Research, 67A*, 172–178.
World Health Organization (WHO). (2015). *The global prevalence of anaemia in 2011*. Geneva: Switzerland, WHO.
Zimmermann, M. (2004). The potential of encapsulated iron compounds in food fortification: A review. *International Journal for Vitamin and Nutrition Research, 74*, 453–461.
Zuidam, N. (2012). An industry perspective on the advantages and disadvantages of iron micronutrient delivery systems. In N. Garti, & D. J. McClements (Eds.), *Encapsulation technologies and delivery systems for food ingredients and nutraceuticals* (pp. 505–540). Cambridge, UK: Woodhead Publishing Ltd.